

What can superconductivity learn from quantized vorticity in ^3He superfluids?

G. E. Volovik^{1,2}, V. B. Eltsov^{1,3}, and M. Krusius¹

¹ Low Temperature Laboratory, Helsinki University of Technology, P.O.Box 2200, FIN-02015 HUT, Espoo, Finland

² Landau Institute for Theoretical Physics, Kosygina 2, 117334 Moscow, Russia

³ Kapitza Institute for Physical Problems, Kosygina 2, 117334 Moscow, Russia

Abstract. In ^3He superfluids quantized vorticity can take many different forms: It can appear as distributed periodic textures, as sheets, or as lines. In the anisotropic $^3\text{He-A}$ phase in most cases the amplitude of the order parameter remains constant throughout the vortex structure and only its orientation changes in space. In the quasi-isotropic $^3\text{He-B}$ phase vortex lines have a hard core where the order parameter has reduced, but finite amplitude. The different structures have been firmly identified, based on both measurement and calculation. What parallels can be drawn from this information to the new unconventional superconductors or Bose-Einstein condensates?

1 Unconventional quantized vorticity

Soon after the discovery of the ^3He superfluids in 1972 it was understood that they represented the first example of unconventional Cooper pairing among Fermi systems, a p-wave state with total spin $S = 1$ and orbital momentum $L = 1$ [1]. This led to a wide variety of new phenomena, of which one of the most important is the discovery of new vortex structures [2]. These can be studied with NMR spectroscopy [3], when this is combined with a calculation of the order parameter texture [4].

In recent years other unconventional macroscopic quantum systems have been found and have taken the centre stage. Intermetallic alloys such as the heavy fermion metals, the high-temperature superconductors, and the most recent addition, the layered superconductors of Sr_2RuO_4 type, do not fit in the conventional picture of s-wave pairing. Is it possible that unconventional vortex structures, similar perhaps to some of those in the ^3He superfluids, might also be present in these new systems?

Current belief holds that the superconducting state in the tetragonal Sr_2RuO_4 material is described by an order parameter of the same symmetry class as that in $^3\text{He-A}$ [5,6], an anisotropic superfluid with uniaxial symmetry (where both time reversal symmetry and reflection symmetry are spontaneously broken). Recent advances in optical trapping and cooling of alkali atom clouds to Bose-Einstein condensates have produced Bose systems which also are described by a multi-component order parameter: The spinor

(ii) If the vortex has a hard core but the order parameter has a finite amplitude everywhere within the core, then we call this a *non-singular* vortex, as is generally done in the literature on unconventional superconductivity. Such a core can be viewed as consisting from a different broken symmetry state than the bulk phase outside the core. Vortices in ${}^3\text{He-B}$ are non-singular: the core of the vortex is made up of some non-B-phase components of the order parameter, either the axial (ie. ${}^3\text{He-A}$) or axiplanar state (Sec. 8). The length scale, which determines the core radius, is $\xi(T, P) \sim 10 - 100 \text{ nm}$.

(iii) The *continuous* vortex has an almost constant order-parameter amplitude throughout the *soft* vortex core. By the soft core we mean a core whose size is much larger than $\xi(T, P)$. Within the soft core primarily the orientation of the order parameter changes. The larger the soft core diameter, the smoother is the distribution of the order-parameter amplitude. Examples of continuous vortices are the *doubly quantized vortex* in ${}^3\text{He-A}$ (Sec. 3) and the vortex in a two-component Bose-Einstein condensate (Sec. 4). In ${}^3\text{He-A}$ the length scale, which determines the soft-core radius, is the healing length of the dipolar spin-orbit interaction: $\xi_D(T, P) \sim 10 - 40 \mu\text{m}$.

(iv) A vortex with a *composite* core has onion structure: It has a hard core (with radius $\sim \xi$), which can be either singular or non-singular, but is embedded within a soft core (with radius $\sim \xi_D$). (a) The *singly quantized vortex* in ${}^3\text{He-A}$ is the prime example (Sec. 5). It has a hard non-singular core within a large soft core. The superfluid circulation is generated by the soft core, but the hard core is needed to satisfy the boundary conditions on the orbital part of the order-parameter field, such that it becomes continuous with respect to the bulk fluid. (b) At high enough magnetic field, the singly quantized vortices in ${}^3\text{He-B}$ have composite cores. Here the vorticity is concentrated in the hard core, while the soft core supports an inhomogeneous order-parameter distribution where the spin-orbit interaction is not minimized. This soft core is a deformation in the order-parameter texture which occurs primarily in the spin part. (c) The *spin-mass vortex* in ${}^3\text{He-B}$ is a composite defect with a narrow hard core, around which the superfluid circulation is trapped. This core is embedded within a planar domain-wall-like soliton defect where the spin-orbit interaction is not minimized and which supports a spin current.

The distinction between non-singular and continuous vortices, and also the existence of a vortex with a composite core rely upon the presence of two length scales, which in turn are determined by two energy scales. In superfluid ${}^3\text{He}$ the two relevant energy scales are the weak spin-orbit interaction and the two orders of magnitude larger superfluid condensation energy. These fix the soft and the hard core sizes, respectively, and as a result the soft core is typically two orders of magnitude larger in diameter than the hard core. If the two scales become comparable in magnitude (as typically occurs in superconductors), then the difference between the continuous and non-singular vortices is washed out.

An understanding of the various structures, in which quantized vorticity may appear, has led to new insight in the physics of macroscopic quantum systems. This new understanding now promises to bring surprising rewards. The discovery of gap nodes in the spectrum of quasiparticle excitations is generally taken to be a signal for unconventional pairing in Fermi systems. An important observation from recent years is the fact that in the vicinity of these gap nodes the energy spectrum is linear and the system acquires all the attributes of relativistic quantum field theory: the analogues of Lorentz invariance, gauge invariance, general covariance, etc. all are present. Therefore fermion superfluids and superconductors on one hand and quantum field theory on the other hand show surprising conceptual similarity. This makes it possible to treat the condensed-matter quantum systems as laboratory models to study physical principles which might also be effective in high energy physics or cosmology. The first examples of such work have been seen in “cosmological” laboratory experiments. For instance, it was recently demonstrated that quantized vortex lines, or linear topological defects as they are known in field theory, are produced in quench-cooled transitions from the normal to the superfluid/superconducting state [7]. This process has been suggested to mimic the production of cosmic strings in Big-Bang expansion. A second effort was related to the dynamics of vortex lines and was exploited to explain the matter-antimatter asymmetry in the Early Universe [8], if it is assumed to result from the axial anomaly of relativistic field theory. Relativistic quantum field theory may just have found itself an unexpected accomplice!

2 Special features of ^3He superfluids

Superfluid ^3He has been blessed with the most ideal properties among the dense coherent quantum systems, approaching those of the alkali atom clouds in Bose-Einstein condensed states: (i) There are no bulk impurities since all alien particles are expelled to the container walls. (ii) The superfluid coherence length $\xi(T, P)$, in addition to being a function of temperature T , also depends on the applied pressure P . By choosing the pressure, the density and interactions can be varied and $\xi(0, P)$ decreases from 65 nm at zero pressure to 12 nm at the liquid-solid transition ($P = 34.4$ bar). (iii) For the best wall materials surface roughness can be reduced close to the level of $\xi(T, P)$. Experimentally this has important consequences, when the container walls approach ideal solid boundaries. (iv) Being an isotropic liquid and a Fermi system, liquid ^3He is theoretically more tractable than either superconductors or liquid ^4He . All complexity and anisotropy is simply derived from the order parameter, with Cooper pairs in p-wave states [9]. In practice this means that experimental observation can be confirmed by detailed theoretical calculation, although often only retrospectively, once the true behaviour is already known.

3 Continuous vortex, skyrmions and merons

One of the most striking results emerging from ^3He research is the existence of vortices with perfectly continuous singularity-free structure. In such a vortex the order-parameter amplitude remains constant throughout the whole structure while its orientation changes in a continuous manner. In the $^3\text{He-A}$ phase with axial anisotropy (and Cooper pairs in $L = S = 1$ states), the orbital order-parameter orientation is denoted by the symmetry axis $\hat{\mathbf{I}}$ which points in the direction of the nodes of the superfluid energy gap. At very low magnetic fields vorticity is distributed over the entire primitive cell of the vortex array and thereby takes the form of a periodic order-parameter texture. At higher fields a region of concentrated vorticity is formed, the soft vortex core. An integral number of phase windings is reached along a closed path which encircles the boundary of the unit cell or the soft core.

The simplest possible vortex structure with continuous vorticity in $^3\text{He-A}$ is the doubly quantized vortex line. In Fig. 2 the orientational distribution of $\hat{\mathbf{I}}$ within the soft vortex core is depicted with arrows. By following their flow, it is noted that all possible 4π directions of the radius vector of the unit sphere are present here. This topology of order-parameter orientations ensures two quanta of circulation ($N = 2$).

The 4π topology of $\hat{\mathbf{I}}$ orientations within the soft core is known as a *skyrmion*. It can be divided into a pair of *merons* [10,11,12] ($\mu\epsilon\rho\sigma$ means fraction [10]), which in the ^3He literature are called Mermin-Ho vortices. In the complete skyrmion the $\hat{\mathbf{I}}$ vector sweeps the whole unit sphere while each meron, or Mermin-Ho vortex, covers only the orientations in one hemisphere and therefore carries one quantum of vorticity ($N = 1$). The meron covering the northern hemisphere forms a circular 2π Mermin-Ho vortex, while the meron covering the southern hemisphere is the hyperbolic 2π Mermin-Ho vortex. The centers of the merons correspond to minima in the potential of trapped spin-wave states, which generate the satellite peak in the NMR absorption spectrum and make the soft cores observable in NMR measurement. The satellite from the doubly quantized vortex was first detected in rotating $^3\text{He-A}$ in 1982 [13], but it is only recently that single-vortex sensitivity was reached and the quantization number $N = 2$ was verified directly [14].

Skyrmions and merons are popular structures in physics: For instance, the double-quantum vortex, in the form of a pair of merons similar to that in $^3\text{He-A}$, is also discussed in the quantum Hall effect where it is formed by pseudo-spin orientations in the magnetic structure [15]. In QCD merons are suggested to produce the color confinement [12].

In superconductors continuous vortices have been discussed in Ref. [16] within a model where the spin-orbit coupling between the electronic spins and the crystal lattice is small and the spin rotation group $SO(3)_S$ is almost exact. The vortex has essentially the same topology as in $^3\text{He-A}$ except that instead of the orbital momentum $\hat{\mathbf{I}}$ it is the spin orientations $\hat{\mathbf{s}}$ of the Cooper pairs which cover a solid angle of 4π in the soft core.

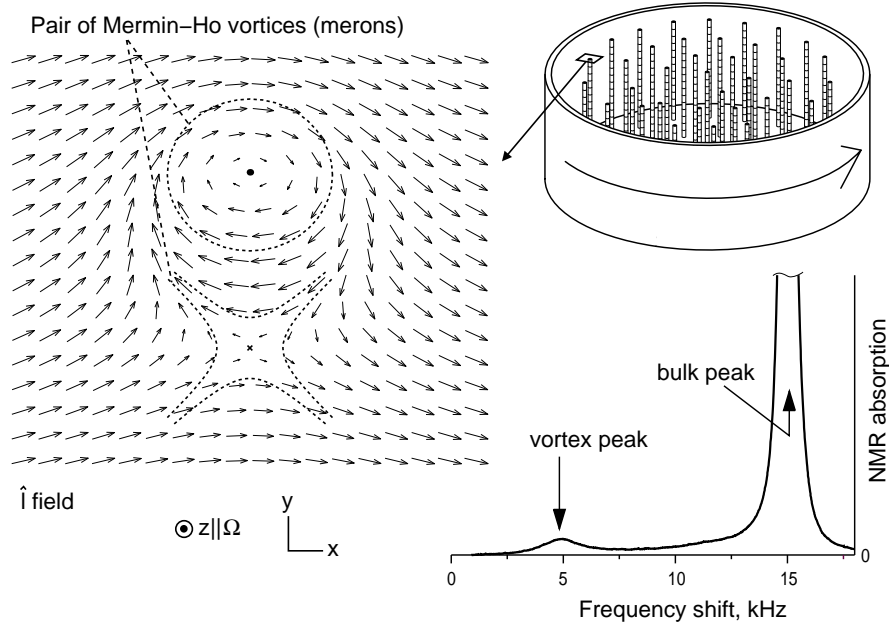


Fig. 2. Doubly quantized vortex line in ${}^3\text{He-A}$ with continuous structure in the soft vortex core: *(Top right)* Rotating container with quantized vortex lines. The pillars depict the soft vortex cores, with a diameter of roughly $80\ \mu\text{m} \gg \xi(T, P)$. Each soft core is encircled by a persistent superfluid circulation of two quanta $2\kappa = h/m_3 = 0.13\ \text{mm}^2/\text{s}$. *(Bottom right)* NMR spectroscopy of topological defects in ${}^3\text{He-A}$. In an external magnetic field, which exceeds the equivalent of the spin-orbit interaction, $H > H_D \approx 3\ \text{mT}$, the spin $\hat{\mathbf{d}}$ and orbital $\hat{\mathbf{l}}$ axes are not aligned parallel in the soft core. Spin-orbit interaction exerts an extra torque on spin precession in nuclear magnetic resonance which shifts the NMR frequency [1]. This torque has different value within and outside the soft core, and thus gives rise to a satellite absorption peak. Both the frequency shift and the absorption intensity of the satellite are characteristic of the order-parameter texture in the soft core [3]. *(Left)* Orientational distribution of the orbital quantization axis $\hat{\mathbf{l}}$ in the soft core, depicted in terms of the projection of $\hat{\mathbf{l}}$ on the plane perpendicular to the vortex axis. The $\hat{\mathbf{l}}$ orientations cover a solid angle of 4π and the distribution is everywhere continuous. This gives rise to a superfluid circulation of two quanta around the soft core.

4 Transformation from singular to continuous vortex

From the topological point of view, all vortices with the same winding number N can be transformed to each other without changing the asymptotic behaviour of the order parameter, simply by reconstruction of the vortex core. To obtain the continuous vortex in ${}^3\text{He-A}$ (Fig. 2) we can start with a $N = 2$ *singular phase vortex*, which has a hard core of the size of the coherence length and a uniformly oriented orbital momentum axis $\hat{\mathbf{l}}$ along $\hat{\mathbf{x}}$.

This is a pure phase vortex for the orbital component $L_x = +1$ of the order parameter, which vanishes only on the vortex axis while other components are zero everywhere. If we now allow for the presence of the other components $L_x = 0$ and $L_x = -1$, then we might fill the hard core with these components, such that the core becomes non-singular. The non-singular core can expand further to form a continuous soft core, which is much larger in radius than the coherence length. Its size is limited by some other weaker energy scales, for instance in $^3\text{He-A}$ by the tiny spin-orbit interaction. Within the core $\hat{\mathbf{l}}$ sweeps through all possible orientations and the topology becomes that of a skyrmion.

This transformation between continuous and singular vorticity has direct application to Bose-Einstein condensates. Suppose a mixture of two sub states can be rotated in a laser manipulated trap. Here one starts with a single Bose-condensate which we denote as the $|\uparrow\rangle$ component. Within this component a pure $N = 1$ phase vortex with singular core is created. Next the hard core of the vortex is filled with the second component in the $|\downarrow\rangle$ state. As a result the core expands and a vortex with continuous structure is obtained. Such a skyrmion has recently been observed with ^{87}Rb atoms [17]. It can be represented in terms of the $\hat{\mathbf{l}}$ vector which is constructed from the components of the order parameter as

$$\begin{pmatrix} \Psi_\uparrow \\ \Psi_\downarrow \end{pmatrix} = |\Psi_\uparrow(\infty)| \begin{pmatrix} e^{i\phi} \cos \frac{\beta(r)}{2} \\ \sin \frac{\beta(r)}{2} \end{pmatrix}, \quad \hat{\mathbf{l}} = (\sin \beta \cos \phi, -\sin \beta \sin \phi, \cos \beta). \quad (1)$$

Here r and ϕ are the cylindrical coordinates with the axis $\hat{\mathbf{z}}$ along the vortex axis. The polar angle $\beta(r)$ of the $\hat{\mathbf{l}}$ vector changes from 0 at infinity, where $\hat{\mathbf{l}} = \hat{\mathbf{z}}$ and only the $|\uparrow\rangle$ component is present, to $\beta(0) = \pi$ at the axis, where $\hat{\mathbf{l}} = -\hat{\mathbf{z}}$ and only the $|\downarrow\rangle$ component is present (Fig. 1). Thus the vector $\hat{\mathbf{l}}$ sweeps the whole unit sphere. As distinct from $^3\text{He-A}$, where the orbital part of the order parameter has three components and the vortex has $N = 2$ circulation, this mixture of Bose-condensates has two components and the continuous vortex has $N = 1$ phase winding. Various schemes have recently been discussed by which a meron with phase winding can be created in a Bose-condensate formed within a three-component $F = 1$ manifold [18,19,20].

5 Vortex with composite core

The singly quantized vortex in $^3\text{He-A}$ has a composite core: It is a $N = 1$ vortex with a non-singular hard core, but where the superfluid circulation is generated by the soft core. Thus this $N = 1$ vortex is not a simple $U(1)$ phase vortex, which would have circulation trapped around a hard core in an otherwise homogeneous $\hat{\mathbf{l}}$ texture. In fact, the function of the hard core is only to provide the topological stability of the soft core, which with its 2π orientational distribution of the $\hat{\mathbf{l}}$ field produces all the vorticity. This

vortex structure has the lowest energy in a magnetic field ($H > 3$ mT) at low rotation velocity ($\Omega \lesssim 1$ rad/s) [21]. Thus it can be created by cooling slowly through T_c in rotation at low Ω , which secures the equilibrium vortex state in an adiabatically slow transition. In contrast, if one starts to rotate the fluid when it is already in the superfluid state below T_c , then the $N = 1$ vortex is generally not formed, because the $N = 2$ vortex has lower critical velocity and is created first. The larger critical velocity of the $N = 1$ vortex reflects the much larger energy barrier involved in the creation of the hard vortex core (Sec. 9.3). Experimentally the singly and doubly quantized vortex lines can be distinguished by their very different NMR absorption satellites.

6 Vortex sheet

6.1 Vortex-sheet structure in $^3\text{He-A}$

In $^3\text{He-A}$ the double-quantum vortex line is not the only unconventional vortex structure with perfect continuity in the order parameter amplitude. The most unusual continuous structure is the *vortex sheet* [22], with planar topology (Fig. 3). It consists of a folded domain-wall-like structure, a soliton sheet, which separates regions with opposite orientations of the $\hat{\mathbf{l}}$ vector. Within this meandering sheet the continuous Mermin-Ho vortex lines with $N = 1$ are confined. These vortices form a chain of alternating circular and hyperbolic merons, which are similar to the two constituents of the soft core in Fig. 2. Each meron represents a kink in the soliton structure and is thus topologically trapped within the soliton: it cannot exist as an independent object in the bulk liquid outside the soliton. An analogous example are Bloch lines within a Bloch wall in ferromagnetic materials. The sheet is attached along two connection lines to the lateral boundaries. It is through these connection lines that merons with $N = 1$ vortex quanta can enter or leave the sheet.

6.2 Vortex sheet in rotating superfluid

The vortex sheet is well known from classical turbulence as a thin interface across which the tangential component of the flow velocity is discontinuous. Within this sheet vorticity approaches infinity while the width of the sheet approaches zero [23]. Historically in superfluids, vorticity was first suggested to be confined to sheets, when Onsager [24] and London [25] described the superfluid state of $^4\text{He-II}$ under rotation. It soon turned out, however, that in $^4\text{He-II}$ a vortex sheet is unstable towards break-up into separated quantized vortex lines. Nevertheless, a calculation on the sheet spacing by Landau and Lifshitz [26], who did not impose a quantization requirement, happens to be exactly to the point for the vortex sheet in $^3\text{He-A}$. Here the vortex sheet proved to be stable owing to the topological confinement of the vorticity within the topologically stable soliton sheet [22].

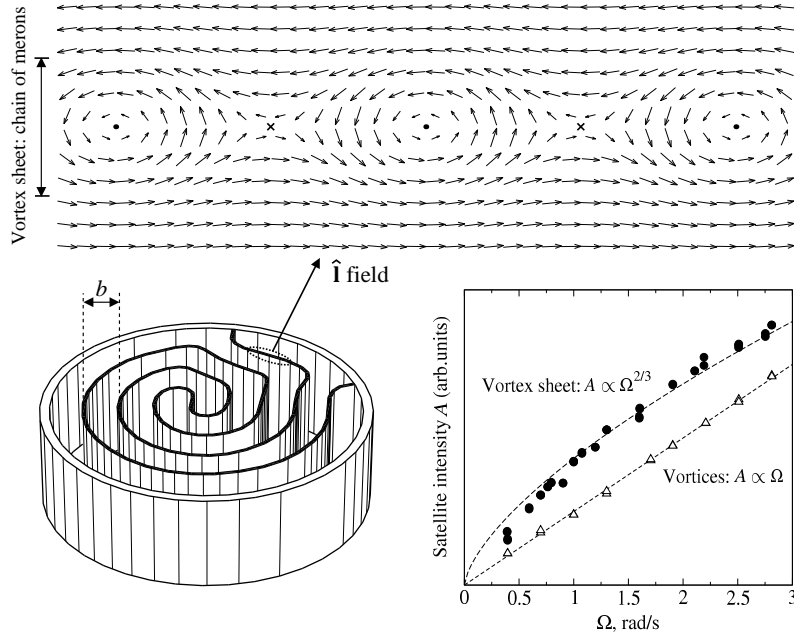


Fig. 3. Vortex sheet in ${}^3\text{He-A}$: (*Bottom left*) The macroscopic configuration of the equilibrium vortex sheet consists of a single continuously folded sheet which fills the rotating container evenly. In an axially oriented external magnetic field the meander forms a double spiral which mimics the original Onsager suggestion of concentric coaxial cylindrical surfaces. (*Top*) Orbital order-parameter texture in the vortex sheet. The arrows depict the projection of $\hat{\mathbf{I}}$ in the xy -plane (perpendicular to the rotation axis Ω). This texture consists of an alternating chain of circular (center marked with black dot) and hyperbolic (center marked with cross) merons. If one follows a path along the centers of merons, the $\hat{\mathbf{I}}$ orientation winds continuously: thus the vorticity is continuously distributed along the sheet. Outside the sheet both $\hat{\mathbf{I}}$ and the counterflow velocity $\mathbf{v} = \mathbf{v}_n - \mathbf{v}_s$ are oriented parallel to the sheet, but in opposite directions on the two sides of the sheet. (*Bottom right*) The integrated NMR absorption in the satellite peak of continuous vortex lines in Fig. 2 follows a linear dependence on the rotation velocity Ω or, equivalently, the number of vortex lines in the equilibrium state of rotation. In contrast, if a soliton sheet preexists in the container and rotation is slowly increased, then a satellite peak with a nonlinear dependence on Ω is grown. This is the signature of the vortex sheet as a rotating state of superfluid.

The equilibrium state of the vortex sheet in a rotating vessel is constructed by considering the kinetic energy from the flow between the folds and the surface tension σ from the soliton sheet. It is then concluded that the distance between the parallel folds has to be $b = (3\sigma/\rho_{s\parallel})^{1/3} \Omega^{-2/3}$. This is somewhat larger than the inter-vortex distance in a cluster of vortex lines. The areal density of circulation quanta has approximately the solid-body value

$n_v = 2\Omega/\kappa$. This means that the length of the vortex sheet per two circulation quanta is $p = \kappa/(b\Omega)$, which is the periodicity of the order-parameter structure in Fig. 3 ($p \approx 180 \mu\text{m}$ at $\Omega = 1 \text{ rad/s}$). The NMR absorption in the vortex-sheet satellite is proportional to the total volume of the sheet which in turn is proportional to $1/b \propto \Omega^{2/3}$. This nonlinear dependence of the satellite absorption on rotation velocity is one of the experimental signatures. Locally the equilibrium vortex sheet corresponds to a configuration with accurately equidistant layers. This is manifested by Bragg reflections of spin waves between the folds of the sheet, which produces a characteristic frequency shifted absorption in the observed NMR line shape [27].

6.3 Vortex sheet in superconductor

The vortex sheet has also been discussed in unconventional superconductors [28,29]. Similar to superfluid $^3\text{He-A}$ the vorticity is trapped in a domain wall which separates two domains with opposite orientations of the $\hat{\mathbf{I}}$ -vector [30]. But, unlike the case of $^3\text{He-A}$, the trapped kink is not a meron but a singular vortex with the fractional winding number $N = 1/2$ (in contrast to isolated vortex lines which are singly quantized). If there are many trapped fractional vortices, then they form a vortex sheet, which as suggested in Ref. [29], can be responsible for the flux flow dynamics in the low-temperature phase of the heavy-fermion superconductor UPt_3 . In superconductors a vortex-sheet-like structure could also appear dynamically, when it is topologically not stable. This state would correspond to a smectic phase of the flowing vortex matter, as was argued in the case of eg. NbSe_2 [31].

7 Fractional vorticity and fractional flux

An unusual object is the *half-quantum vortex*. Here the order-parameter phase changes by π on circling once around this line. The change of sign of the order parameter can be compensated by some extra degree of freedom, which usually is the spin. Such a linear structure was originally predicted to appear in $^3\text{He-A}$ [32], but has not yet been observed there experimentally. Later it was also predicted to appear in unconventional superconductors [33]. Some years ago it was discovered as the intersection line of three grain boundary planes in a thin film of $\text{YBa}_2\text{Cu}_3\text{O}_{7-\delta}$ [34]. The half-quantum vortex has also been suggested to exist in Bose-Einstein condensates with a hyperfine spin $F = 1$ [35].

Based on the $^3\text{He-A}$ example more possible structures of the fractional vortices in unconventional superconductors can be predicted. In $^3\text{He-A}$ the discrete symmetry, which supports the half-quantum vortex, arises from the changes in sign when the spin axis $\hat{\mathbf{d}}$ and the orbital axis $\hat{\mathbf{e}}_1 + i\hat{\mathbf{e}}_2$ are taken

once around the line and rotate into $-\hat{\mathbf{d}}$ and $-(\hat{\mathbf{e}}_1 + i\hat{\mathbf{e}}_2)$. When both of these axes change sign, then the order parameter returns to its initial value

$$\hat{\mathbf{d}} = \hat{\mathbf{x}} \cos \frac{\phi}{2} + \hat{\mathbf{y}} \sin \frac{\phi}{2} \quad , \quad \hat{\mathbf{e}}_1 + i\hat{\mathbf{e}}_2 = (\hat{\mathbf{x}} + i\hat{\mathbf{y}})e^{i\phi/2} \quad . \quad (2)$$

Here ϕ is the azimuthal angle of the cylindrical coordinate system and the magnetic field is applied along $\hat{\mathbf{z}}$ to keep $\hat{\mathbf{d}}$ in the xy plane. The spin axis $\hat{\mathbf{d}}$ rotates by π on circling around the half-quantum vortex. Thus a ‘‘spectator’’ in $^3\text{He-A}$, who travels around the vortex, would find its spin reversed with respect to the spin of a ‘‘spectator’’ who was at rest. This situation is the analog of the Alice string in particle physics [36] where a particle, which moves around the string, in a continuous manner flips its charge or parity or enters the ‘‘shadow’’ world [37].

In superconductors the crystalline structure must be taken into account. In the simplest representation which preserves tetragonal symmetry, the p -wave order parameter in Sr_2RuO_4 has the form

$$\Delta(\mathbf{k}) = \Delta_0 (\hat{\mathbf{d}} \cdot \boldsymbol{\sigma}) (\sin \mathbf{k} \cdot \mathbf{a} + i \sin \mathbf{k} \cdot \mathbf{b}) e^{i\theta} \quad , \quad (3)$$

where \mathbf{k} is momentum, θ is the phase of the order parameter, \mathbf{a} and \mathbf{b} are the elementary vectors in the basal plane of the crystal lattice. Vortices with fractional quantization N can now be constructed in two ways. If the $\hat{\mathbf{d}}$ -field is sufficiently flexible, the analog of the vortex with $N = 1/2$ in Eq. (2) becomes possible, where $\hat{\mathbf{d}} \rightarrow -\hat{\mathbf{d}}$ and $\theta \rightarrow \theta + \pi$ on circling once around the vortex [38]. Another possibility is the Möbius-strip geometry. Here the crystal axes \mathbf{a} and \mathbf{b} are twisted continuously by the angle $\pi/2$ on traversing around the closed wire loop [39]. This closed loop traps fractional flux, since the local orientation of the crystal lattice continuously changes by $\pi/2$ around the loop, $\mathbf{a} \rightarrow \mathbf{b}$ and $\mathbf{b} \rightarrow -\mathbf{a}$, which means that the order parameter becomes multiplied by i . The single-valuedness of the order parameter requires that this change must be compensated by a change in the phase θ by $\pi/2$. As a result the phase winding around the loop is $\pi/2$ and $N = 1/4$.

This, however, does not mean that such a Möbius loop in a chiral p -wave superconductor traps $1/4$ of the magnetic flux Φ_0 of a conventional Abrikosov vortex. Because of the breaking of time reversal symmetry in chiral crystalline superconductors, persistent electric currents arise not only due to phase coherence but also due to deformations of the crystal [40]:

$$\mathbf{j} = \rho_s \left(\mathbf{v}_s - \frac{e}{mc} \mathbf{A} \right) + K a_i \nabla b_i \quad , \quad \mathbf{v}_s = \frac{\hbar}{2m} \nabla \theta \quad . \quad (4)$$

The magnetic flux trapped in the loop is obtained from the condition of zero current, $\mathbf{j} = 0$ in Eq. (4). Thus, the trapped flux depends on the parameter K in the deformation current. In the limiting case of $K = 0$ the flux is $\Phi_0/4$ (or $\Phi_0/6$ if the underlying crystal lattice has hexagonal symmetry).

In a nonchiral d -wave superconductor of layered cuprate-oxide structure the order parameter can be represented by:

$$\Delta(\mathbf{k}) = \Delta_0 (\sin^2 \mathbf{k} \cdot \mathbf{a} - \sin^2 \mathbf{k} \cdot \mathbf{b}) e^{i\theta} . \quad (5)$$

The same twisted wire loop which transforms $\mathbf{a} \rightarrow \mathbf{b}$ and $\mathbf{b} \rightarrow -\mathbf{a}$, produces a change of sign of the order parameter, which must be compensated by a change of the phase θ by π . This corresponds to a circulation of half a quantum $N = 1/2$, i.e. the fractional flux trapped by this loop is $\Phi_0/2$, since the parameter K in Eq. (4) is exactly zero in nonchiral superconductors. The same reasoning gives rise to the $\Phi_0/2$ flux associated with the intersection line of three grain boundary planes, the tri-crystal line [34]: around this line $\mathbf{a} \rightarrow \mathbf{b}$ and $\mathbf{b} \rightarrow -\mathbf{a}$. Only the observation of a fractional flux different from $\Phi_0/2$ would indicate the breaking of time reversal symmetry [28,40,41].

8 Broken symmetry in the vortex core

In the quasi-isotropic $^3\text{He-B}$ phase (with Cooper pairs in the total angular momentum state $J = 0$), the simplest possible vortex is a singular vortex with $N = 1$, where all the order-parameter components are zero on the axis of the vortex core. However, this vortex is never realized. All vortices (and other linear defects) observed in $^3\text{He-B}$ have a non-singular hard core. This is a typical situation for superfluids/superconductors with a multi-component order parameter. As a rule the superfluid/superconductor does not tolerate a full suppression of the superfluid fraction in the core, if there is a possibility to escape this by filling the core with other components of the order parameter. This rule applies also to high-temperature superconductors with d -wave pairing, where the $N = 1$ vortex supports a nonzero s -wave component in the vortex core [42].

8.1 Vortex core transition

The first NMR measurement on rotating $^3\text{He-B}$ revealed as a function of temperature and pressure a first order phase transition in the vortex core structure [43]. This phenomenon in Fig. 4 was the first example of a phase transition in the structure of any topological defect. Other transitions have been identified in $^3\text{He-A}$ since then, but the B-phase transition remains the most prominent one. This transition separates two vortices with the same topology ($N = 1$), but with a different structure of the hard core. The existence of the transition illustrates that vortices in $^3\text{He-B}$ have to be non-singular and have a complex structure of the hard core. Later these two stable vortex core structures were theoretically identified as two different stationary minimum energy solutions as a function of pressure in the Ginzburg-Landau temperature regime. Both structures have broken parity in the core.

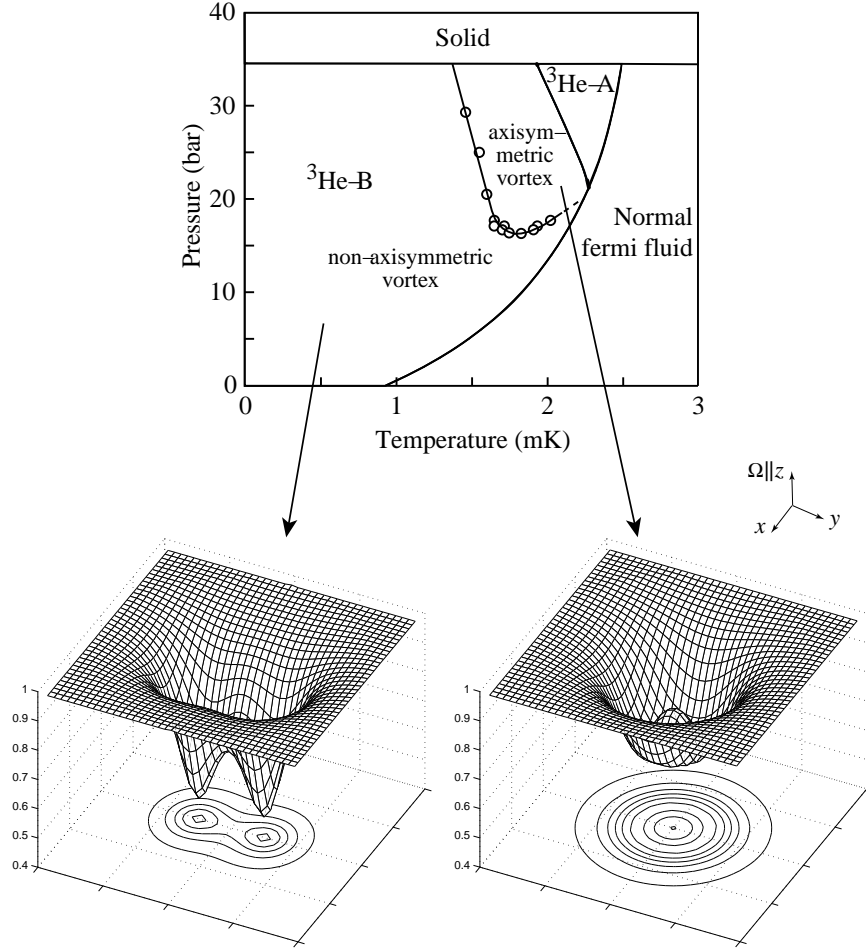


Fig. 4. Phase transition in the structure of the singular vortex core in $^3\text{He-B}$: (*Top*) Pressure vs. temperature phase diagram of ^3He liquids, with the phase transition line for the B-phase vortex core structure. The exact intercept of the transition line at T_c is unknown. (*Bottom*) Both measurement [45] and calculation [46] confirm that the axisymmetric core at high temperatures spontaneously reduces its symmetry and transforms to a double-well structure at low temperatures. The magnitude of the square of the order-parameter amplitude has here been plotted in the xy -plane (perpendicular to the rotation axis) for the two core structures. This quantity remains finite throughout the cross section of the core.

8.2 Ferromagnetic core

The high-pressure $^3\text{He-B}$ vortex has an axis-symmetric core in which the A-phase order-parameter components dominate. These components produce in-

crease in the order parameter amplitude close to vortex axis which is shown in Fig. 4, bottom right. This non-singular vortex with a superfluid core lies lower in energy, than the simplest most symmetric solution with a normal core, and displays ferromagnetic spin polarization [44], which is observed in the rotating NMR experiments as a gyromagnetism [45].

Similar, but antiferromagnetic cores have been discussed for high- T_c vortices within the popular $SO(5)$ model for superconductivity and antiferromagnetism [47]. Here it has been established that in the Ginzburg-Landau regime, in certain regions of the parameter values, a solution with normal vortex cores is unstable with respect to non-singular antiferromagnetic cores [48]. Also non-singular vortex cores in the heavy fermion superconductor UPt_3 could possibly explain why a three times larger flux-flow resistivity is observed parallel to the \hat{c} axis compared to the perpendicular directions [49].

8.3 Asymmetric double core

The low-temperature B-phase vortex has a non-axisymmetric core, i.e. the axial $U(1)$ symmetry of the ferromagnetic core is spontaneously broken, to create a dumbbell-like double core (Fig. 4, bottom left). It can be considered as a pair of half-quantum vortices, connected by a non-topological wall [2,46,51]. The separation of the half-quantum vortices increases with decreasing pressure and thus the two-core structure is most pronounced at zero pressure [52]. The asymmetry of the core has been verified by direct observation of a Goldstone mode which is a direct consequence from the loss of axial symmetry: the deformed vortex core can become twisted in the presence of a special type of B-phase NMR mode, which is then detected as a reduction in rf absorption [50].

Related phenomena are also possible in superconductors. In Ref. [53] the splitting of the vortex core into a pair of half-quantum vortices has been discussed in heavy-fermion superconductors. In fact a vortex-core splitting may have been observed in high- T_c superconductors [54]. These observations were interpreted as tunneling of a vortex between two neighboring sites in the potential wells created by impurities. However, the phenomenon can also be explained in terms of vortex-core splitting.

9 Vortex formation by intrinsic mechanisms

In addition to vortex structure, the second most important question becomes the creation of the different forms of vorticity. Vortex formation by intrinsic mechanisms is a topic which has been discussed for decades in superfluidity, but which has been notoriously difficult. The problems are caused by interference from extrinsic effects, primarily from remanent vorticity trapped on rough surfaces. One of the major developments from the last ten years has been the emergence of reliable measurements on critical velocities in $^4\text{He-II}$.

These have been performed by monitoring the superflow through sufficiently small sub-micron-size orifices [55,56]. Intrinsic vortex formation has thereby become an important phenomenon in superfluids – quite unlike in superconductors, where typically vortices appear due to different types of extrinsic effects at the lower critical field H_{c1} . However, it is useful even in the case of superconductors to keep in mind the more ideal properties of vortex formation. Also the process of unpinning of vortices which is important for a problem of vortex creep in superconductors can be discussed in terms of vortex nucleation: The motion of vortex from the pinning site is equivalent to creation of a vortex loop which annihilates the pinned part of the vortex line.

9.1 Nucleation barrier

Many vortex phenomena, not only nucleation, but also the unpinning of remanent vorticity, involve energy barriers which are usually overcome by thermal activation. At the lowest temperatures quantum tunneling has been suggested as a possible mechanism, where a macroscopic amount of matter is assumed to participate coherently in a tunneling process. Vortex nucleation in orifice-flow of $^4\text{He-II}$ displays a characteristic low-temperature plateau in the temperature dependence of the critical velocity which has been claimed to support the quantum tunneling concept [57]. This question is also discussed in superconductors in the context of unpinning and creep. However, firm proof for such interpretation is still missing.

In $^3\text{He-B}$ the critical velocity was measured in rotating experiments with single-vortex resolution in the early 1990's. This proved to be a more straightforward measurement than in $^4\text{He-II}$. The measured temperature dependence of the critical velocity resembles that of the superfluid energy gap $\Delta(T, P)$ [58], which at the lowest temperatures also approaches a temperature-independent plateau. The explanation here, however, does not involve quantum tunneling, but the superflow instability. This phenomenon resembles a second order transition where the energy barrier goes to zero as a function of the scanned variable, in this case the superflow velocity.

When a cylinder with superfluid $^3\text{He-B}$ is slowly accelerated to rotation, the state with one single vortex line becomes energetically favorable when the superflow at the circumference exceeds the Feynman critical velocity $v_{c1} = \kappa/(2\pi R) \ln(R/r_c)$ [59]. With a container radius R of a few millimeters and a circulation quantum $\kappa = h/(2m_3) = 0.066 \text{ mm}^2/\text{s}$, this velocity is only 10^{-2} mm/s . Above this velocity remanent vorticity, which has been trapped on the cylinder wall, may start to unpin and then to expand to rectilinear vortex lines. It is the equivalent of H_{c1} in superconductors. However, if we exclude extrinsic mechanisms of vortex formation, then the vortex-free state will persist metastably to much higher velocities because of the nucleation barrier.

In $^3\text{He-B}$ the nucleation barrier is practically impenetrable. The argument is the following: The vortex is nucleated on the wall as a segment of a vortex

ring. The radius of a ring sustained by superflow at the velocity v_s can be written as $r_o = (\kappa/4\pi v_s) \ln(r_o/r_c)$, where the vortex-core radius r_c is of the order of the superfluid coherence length $\xi_{3\text{He}} \sim 10 - 100$ nm. The energy of a ring is $E(v_s) = \frac{1}{2} \rho_s \kappa^2 r_o \ln(r_o/r_c)$, where $\rho_s \sim m/a^3$ is the superfluid density, and a the interatomic distance. This energy constitutes the nucleation barrier. On dimensional grounds we may write $E(v_s)/k_B T \sim (r_o/a)(T_F/T) \ln(r_o/r_c)$, where $T_F = \hbar^2/2ma^2 k_B \sim 1$ K is the degeneracy temperature of the ^3He quantum fluid. Assuming that $r_o > r_c$, we find $E(v_s)/k_B T > 10^5 \ln(r_o/r_c)$. Such a barrier height in $^3\text{He-B}$ is inaccessible at all temperatures below T_c . In contrast in $^4\text{He-II}$, $\xi_{4\text{He}} \sim a$, and the barrier is low, $E(v_s)/k_B T > \ln(r_o/r_c)$. It can be thermally overcome, except at the lowest temperatures below 0.2 K.

9.2 Vortex formation in a hydrodynamic instability

The huge barrier in $^3\text{He-B}$ means that the vortex formation mechanism cannot be thermal activation. When the superflow velocity is increased (by increasing the rotation) a threshold v_{cb} is finally reached above which homogeneous flow loses local stability. This occurs when the energy density of the superflow, $\rho_s v_s^2/2$, exceeds the energy responsible for the topological stability of a vortex, which is of order $\rho_s (\kappa/2\pi r_c)^2$. An order of magnitude estimate of the maximum velocity is thus $v_{cb} \sim \kappa/2\pi r_c$. At this velocity, the radius r_o of the nascent ring becomes comparable to r_c and the nucleation barrier goes to zero. The instability inevitably leads to the creation of a vortex when no other mechanism is available at lower v_s .

In $^4\text{He-II}$ well below T_λ , the estimate of v_{cb} in the form $\kappa/2\pi\xi_{4\text{He}}$ agrees in order of magnitude with the Landau velocity, defined by the roton gap Δ_r and momentum p_r as $v_L = \Delta_r/p_r \sim 60$ m/s [59]. However, this limiting velocity is not observed directly in the measurements of orifice flow, by extrapolating the thermally activated process to $T \rightarrow 0$. The reason is that the measured quantity is the average flow velocity through the aperture and not the local critical velocity at the nucleation site. On the circumference of the orifice, the local velocity will be enhanced from the average value by surface roughness, in particular when the superflow is deflected around any sharp protuberances which match the length scale r_o of the evolving vortex half ring. The most effective of such excrescences on the circumference will then selectively become the nucleation center [58]. For this reason the measured critical velocity is expected to be roughly a factor of $\lesssim 10$ smaller than the ideal limiting value (Fig. 5).

In $^3\text{He-B}$, the estimate of $v_{cb} \sim \kappa/2\pi\xi_{3\text{He}}$ is smaller by 3 orders of magnitude than in $^4\text{He-II}$, but again comparable to the appropriate Landau limit, defined by the energy gap and the Fermi momentum as $\Delta(T)/p_F$. In this case the velocity v_{cb} is also known from direct calculations of the stability limit of homogeneous superflow [60]. As in orifice flow, the measured average velocity at vortex formation is smaller than the calculated bulk v_{cb} and depends on surface roughness. The principal difference from $^4\text{He-II}$ is the much

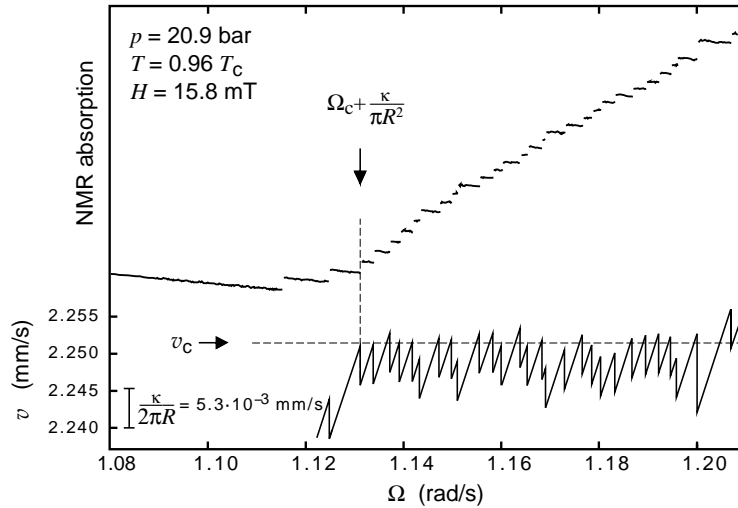


Fig. 5. Single-vortex formation as a function of rotation velocity $\Omega(t)$, for ${}^3\text{He-B}$ in a cylindrical container. *Top:* The vertical axis denotes the height of a NMR absorption peak, where the intensity increases per each newly added vortex line by a constant amount. Vortex formation starts with a first step increase at $\Omega_c = 1.115$ rad/s, but the critical threshold is identified from the third step (dashed vertical line) where the maximum flow velocity v_c reaches a stable value (dashed horizontal line in the plot at bottom). *Bottom:* The corresponding superflow velocity $v_s(R)$ at the cylinder wall. Each step increase in the upper plot corresponds to a drop by $\kappa/(2\pi R)$ in the velocity $v_s(R)$, the equivalent of one circulation quantum $\kappa = h/(2m_3) = 0.066$ mm²/s. The average of the maximum velocities v_s defines the critical velocity v_c . The scatter from the average is probably of experimental origin. The rotation is here increased at a constant slow rate ($d\Omega/dt = 2 \cdot 10^{-4}$ rad/s²), the sample is contained in an epoxy-resin-walled cylinder with radius $R = 2$ mm at a pressure $P = 20.9$ bar, in a magnetic field $H = 15.8$ mT, and temperature $T = 0.96 T_c$. (From Ref. [58].)

larger length scale $r_o \sim \xi_{3\text{He}}$, which means that experimentally the influence of surface roughness is less prominent, remanent vorticity can be avoided in the presence of sufficiently smooth surfaces, and stable periodic vortex formation can be investigated with bulk liquid flowing past a flat wall. This is in stark contrast to ${}^4\text{He-II}$, where the coherence length is of atomic size, surface roughness generally provides an unlimited source of trapped remanent vorticity, and intrinsic nucleation can only be observed in flow through a sufficiently small orifice.

Owing to the excessively high nucleation barrier, in ${}^3\text{He-B}$ it must be the velocity v_{cb} of superflow instability which becomes the appropriate velocity of vortex formation. The process then corresponds to a classical instability, which occurs at the pair-breaking velocity. Thus in the case of ${}^3\text{He-B}$, the

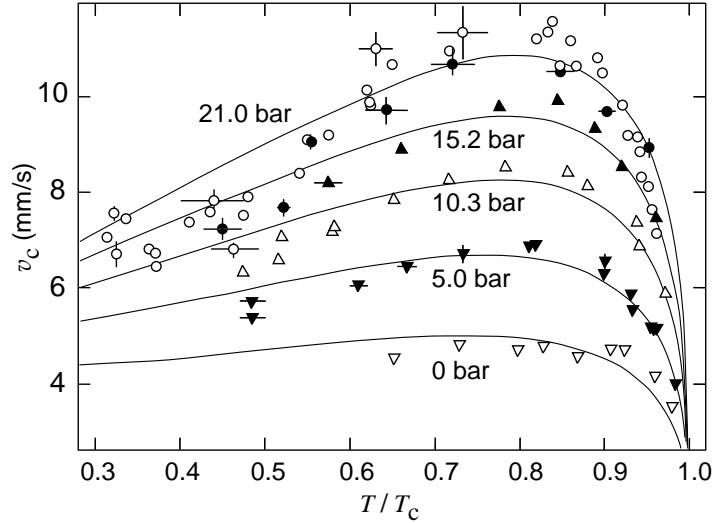


Fig. 6. Measurement of critical flow velocity v_c in ${}^3\text{He-B}$ vs. temperature for pressures $P \leq 21$ bar. The solid curves have been fitted to the data with $v_c = v_{cb}(\xi/d)^\chi$, where the fitting parameters d and χ characterize the surface roughness on the cylinder wall, $v_{cb}(T, P)$ is the calculated bulk liquid superflow instability [60] and $\xi(T, P) = \xi(0, P)[\Delta(0)/\Delta(T)]$ the superfluid coherence length. The roughness is modeled by the protuberance with height d and apex angle $\pi/(1 - \chi)$ which acts as the nucleation center. The fit gives $d = 3.1 \mu\text{m}$ and $\chi = 0.45$ (apex angle $\approx 30^\circ$). The measurements have been performed with an epoxy-resin-walled container with radius $R = 3.5$ mm. (From Ref. [58].)

reason for a plateau in $v_c(T)$ in the $T \rightarrow 0$ limit is that the characteristic physical quantities, such as the gap amplitude $\Delta(T)$, which determine the instability velocity, become temperature independent. Consequently not only quantum tunneling, but also the intrinsic instability provides an explanation for the low-temperature plateaus which are observed in many different systems, including the case of ${}^4\text{He-II}$ at the lowest temperatures.

9.3 Formation of continuous vortex lines: Dependence of critical velocity on core size

The order-of-magnitude expectation for the bulk superflow instability is $v_c \sim \kappa/(2\pi r_c)$, where r_c is the core size of the emerging vortex. For ${}^4\text{He-II}$ and ${}^3\text{He-B}$ it is the size of the hard core, which is on the order of the superfluid coherence length. For the continuous vortex in ${}^3\text{He-A}$ the length scale of the soft core structure is much larger: It is the healing length $\xi_D \gtrsim 10 \mu\text{m}$ of the spin-orbit coupling (Fig. 2). The same length scale also applies to the structure of the soliton and vortex sheets. Because of this long length scale the measured critical velocities in the A phase are two orders of magnitude lower

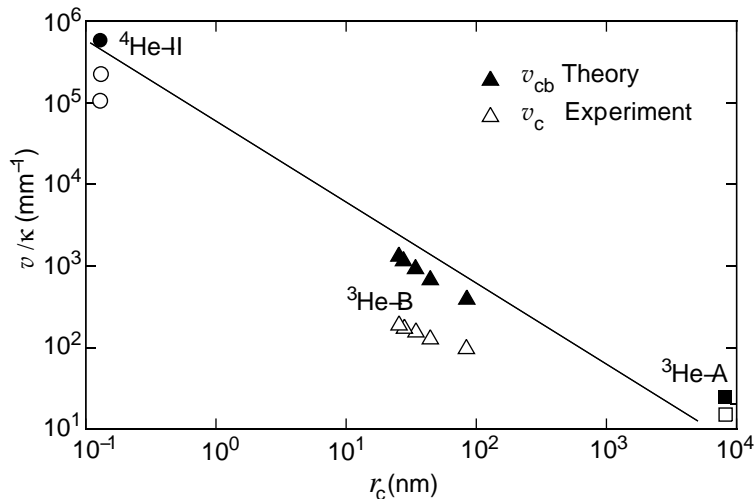


Fig. 7. Theoretical v_{cb}/κ and maximum experimental $v_{c,max}/\kappa$ plotted for 3 superfluids as a function of their core size r_c . For r_c we use 0.1 nm in $^4\text{He-II}$, in $^3\text{He-B}$ it is the superfluid coherence length $\xi(T, P)$, and for continuous vortices in $^3\text{He-A}$ in a magnetic field the spin-orbit healing length ξ_D . In $^4\text{He-II}$ we use the Landau limit v_L for v_{cb} , in $^3\text{He-B}$ v_{cb} is the calculated maximum superflow velocity [60], and in $^3\text{He-A}$ it corresponds to the helical textural instability [61,62]. For $v_{c,max}$ in $^4\text{He-II}$ the measured value in Ref. [57] is used, for $^3\text{He-B}$ data from Ref. [58], and for $^3\text{He-A}$ from Ref. [61]. The line is a guide for the eye, but it obeys the relation $v_c/\kappa \propto 1/r_c$. (From Ref. [58])

than in the B phase, as shown in Fig. 7. This explains why the continuous $N = 2$ vortex is formed in the A liquid when it is accelerated into rotation, rather than the composite $N = 1$ vortex with a hard core, although the latter might be energetically preferred.

At the container wall the boundary condition on the order parameter requires that the orbital quantization axis $\hat{\mathbf{l}}$ has to be oriented along the surface normal. Therefore the center of vortex formation must evolve outside a surface layer with a width $\sim \xi_D$, out of the influence of surface roughness. This has been recently experimentally confirmed [14]. Here the only mechanism available is an instability of the order-parameter texture.

An example of a critical process, which exemplifies the fact that the order-parameter texture is involved, is shown in Fig. 8. Here the vertical axis is the peak height of the satellite absorption in Fig. 2, which is proportional to the number of vortex lines, and the horizontal axis is the external drive. Initially on increasing Ω , no vortex lines are formed. When the critical velocity Ω_c^* is reached, a large number of vortex lines is suddenly simultaneously formed. During further increase of Ω the system recovers and a characteristic linear slope is retrieved. The linear dependence represents a reproducible periodic

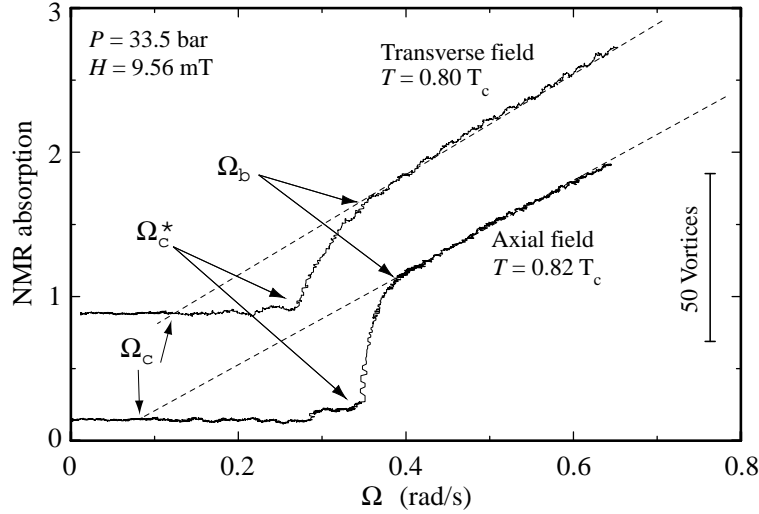


Fig. 8. Two examples of vortex-line formation in a transition of the order-parameter texture in ${}^3\text{He-A}$ as a function of the applied rotation Ω . The texture transition occurs at Ω_c^* , where a large number of vortex lines is simultaneously formed. After the transition in the transformed texture the regular periodic vortex formation process sets in, where the flow is limited by a constant critical velocity $v_c = \Omega_c R$. This process gives a linear dependence for the number of vortex lines \mathcal{N} as a function of Ω , with the slope $d\mathcal{N}/d\Omega = 2\pi R^2/\kappa$.

process where one vortex at a time is formed at a constant critical velocity, similar to that for B-phase vortices in Fig. 5. The extrapolation of the linear dependence back to zero vortex number gives for the onset a lower value Ω_c than the actual initially measured Ω_c^* at the sudden jump. This is an example where the global order parameter texture becomes unstable in the increasing superflow and finally a first order transition occurs in the texture to a new configuration with a lower critical velocity. It is also clear evidence for the fact that the value of the critical velocity depends on the global order parameter texture in the rotating container.

Measurements [61] and calculations [62] of the critical velocity in ${}^3\text{He-A}$ show that the maximum limit for the critical velocity is reached with an ordered texture which mimics one where $\hat{\mathbf{l}}$ is homogeneously oriented along the superflow \mathbf{v}_s . The minimum velocity, in turn, is close to an order of magnitude smaller and is obtained within a soliton sheet where the spin-orbit coupling is broken and the $\hat{\mathbf{l}}$ texture is inhomogeneous.

9.4 Formation of vortex sheet

The dependence of the critical velocity on the core size explains why vorticity with continuous singularity-free structure is formed, when ${}^3\text{He-A}$ is

accelerated to rotation. But is it created in the form of lines or sheets? This has turned out to be an interesting question of general validity. The vortex sheet is formed whenever a vertical dipole-unlocked soliton sheet is present in the container, while rotation is started. Here the critical velocity is the lowest possible, ie. the energy barrier for adding more merons into the sheet vanishes at lower velocity than for any other type of vortex structure.

The critical velocity of the vortex sheet is made up of several contributions. First of all there is the low critical velocity at the connection lines between the sheet and the cylinder wall, where the spin-orbit coupling is broken. Some low superflow velocity is required even here, since at least the attractive interaction of the emerging meron with its image within the wall has to be overcome. A second contribution is a small, but nonzero resistance of the texture in the soliton connection line to reach the instability limit. These small contributions at the connection line are the only ones which are effective initially when rotation is started and the first circulation quanta enter the sheet.

As the sheet grows, a second contribution becomes effective. When a new meron is added, it experiences repulsion from the meron which already resides in the sheet close to the connection line. The repulsion depends on the distance between the merons in the sheet and the sheet's resistance to change its folding and the distribution of circulation in the container. Thus the critical velocity becomes Ω -dependent. At low Ω , when the merons are rare, this contribution is much below the critical velocity for the formation of isolated vortex lines or skyrmions. It was suggested and later experimentally confirmed that the critical velocity follows the qualitative dependence $v_c^*(\Omega) \propto \sqrt{\Omega}$ as shown in Fig. 9. (The star as a superscript marks the fact that v_c^* is obtained from the measured value of Ω_c through the relation $v_c^* = \Omega_c/R$ which is strictly valid only for an axially symmetric distribution of vorticity.)

The vortex sheet has unusual dynamic properties which make it to the preferred state if the rotation drive is rapidly changing in time [63]. It is expected that analogous features can evolve in anisotropic p-wave superconductors with periodic vortex flow in the unpinned regime [64]. The dynamic response of $^3\text{He-A}$ as a function of the frequency and amplitude of the external drive is currently under study [65]. The time proven method to create the vortex sheet is to apply sinusoidally modulated rotation in the form $\Omega = \Omega_1 \sin \omega t$, where the period of modulation is of order $2\pi/\omega \sim 10$ s and the amplitude $\Omega_1 \sim \hbar/(2m_3\xi_D R) \sim 0.3$ rad/s exceeds that required for breaking the spin-orbit coupling. To grow the equilibrium vortex sheet, one applies the oscillating rotation until the signal from the vortex sheet is observed [22]. The final step is to increase Ω from zero to the desired value, using slow acceleration ($d\Omega/dt \lesssim 10^{-3}$ rad/s²) to ensure adiabatic growth of a single folded sheet.

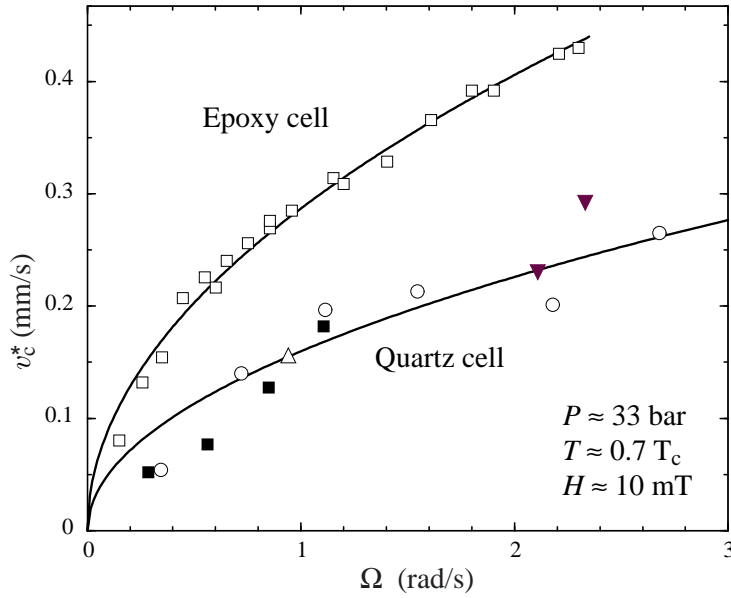


Fig. 9. Critical velocity v_c^* of the adiabatically grown vortex sheet as a function of applied rotation Ω : This state consists of a single sheet, which in an axially oriented magnetic field is folded into a double spiral, as shown in Fig. 3. The solid curves are fits to the measured data with the dependence $v_c^* \propto \sqrt{\Omega}$. An epoxy container with surface roughness of order $10 \mu\text{m}$ displays a larger magnitude of v_c^* than a container with fused quartz walls and an order of magnitude smaller roughness ($\lesssim 1 \mu\text{m}$). The difference could arise from slight pinning of the two connection lines of the sheet along the cylindrical wall which would resist readjustments when new vorticity is added into the sheet during acceleration. The different symbols of data points (quartz cylinder) illustrate the reproducibility of the results from one adiabatically grown vortex sheet to another.

9.5 Vortex formation in ionizing radiation

In the metastable regime of superflow at $v_s < v_c$, vortex formation can be triggered by irradiation with ionizing radiation. Experiments with superfluid $^3\text{He-B}$ [7] have shown that quantized vortex lines are formed in the aftermath of a neutron absorption event. According to current belief, vortex formation occurs via the Kibble-Zurek (KZ) mechanism [66,67], which was originally developed to explain the phase transitions of the Early Universe. In this scenario a network of cosmic strings is formed during a rapid non-equilibrium second order phase transition, owing to thermal fluctuations. In ^3He the absorption of a thermal neutron causes heating which drives the temperature in a small volume of $\sim 100 \mu\text{m}$ size above the superfluid transition. Subsequently the heated bubble cools back below T_c with a thermal relaxation time of order $1 \mu\text{s}$. This process forms the necessary conditions for the Kibble-Zurek mech-

anism within the cooling bubble. It is interesting to note that so far this is the only case of vortex formation in the ^3He superfluids which in principle is not confined to the vicinity of the bounding solid walls. In practice the mean free path of thermal neutrons in liquid ^3He is only $100\ \mu\text{m}$ and therefore even this process is localized close to the wall.

The real experimental conditions in the neutron irradiation experiment of $^3\text{He-B}$ [68] (and also probably in the early Universe) do not coincide, with a perfectly homogeneous transition, as is assumed in the KZ scenario: The temperature distribution within the cooling “neutron bubble” is nonuniform, the transition propagates as a phase front between the normal and superfluid phases, and the phase is fixed outside the bubble. These considerations require modifications to the original KZ scenario [69,70,71] and even raise concerns whether the KZ mechanism is responsible for the defects which are extracted from the neutron bubble and observed in the experiment [72,73]. New measurements demonstrate that a joint defect – the combination of a conventional (mass) vortex and spin vortex – is also formed and is directly observed in the neutron irradiation experiment [74]. This strengthens the importance of the KZ mechanism and places further constraints on the interplay between it and other competing effects.

In superconductors localized heating can cause the unpinning of vortices from defects in the crystal lattice which can be viewed as a creation of an intermediate vortex ring.

10 Vortex dynamics without pinning

As a liquid free of alien impurities, He superfluids do not display bulk pinning. Surface pinning at protuberances on the container wall remains an issue which has been studied in $^4\text{He-II}$ [75]. In ^3He superfluids vortex core diameters are at least two orders of magnitude larger and pinning correspondingly weaker. Measurements of vortex dynamics have so far not resulted in reliable estimates for pinning parameters. In fact, it has not been settled whether surface pinning plays any observable role in the presence of smooth walls. All indications point in the direction that, even in $^3\text{He-B}$ with its smaller vortex core sizes, vortex motion occurs in the limit of weak pinning [76], where collective effects are expected to dominate in pinning. For vortex lines with continuous structure in $^3\text{He-A}$ pinning is expected to be unimportant. The virtual absence of pinning has a number of important consequences:

(i) It allows investigation of vortex dynamics without pinning in the whole temperature range from $T = 0$ to $T = T_c$. As a result, in $^3\text{He-B}$ three topologically different contributions to vortex dynamics have been distinguished from one another, owing to their different temperature behavior [77]. These are 1) the Magnus force with which the flowing superfluid component acts on a vortex line, 2) the Kopnin force which is caused by the spectral flow phenomenon [78] and which acts on the vortex line when it moves with respect

to the normal component, and 3) the Iordanskii force which is the analog of the gravitational Aharonov-Bohm effect [79].

(ii) It becomes possible to prepare surfaces with specially prepared pinning sites by micro-fabrication techniques. One can then study vortex dynamics when an array of vortex lines becomes commensurate with a pre-fabricated lattice of surface pinning sites.

(iii) One can study the trapping and unpinning of circulation from a columnar defect in the order-parameter field – namely a thin wire stretched across the superfluid bath parallel to the rotation axis. This is the Vinen vibrating wire configuration where one quantum of circulation can be trapped around the wire by rotating the container [80]. When rotation is stopped, the trapped circulation can be observed to peel off from the wire as a precessing vortex [81]. With each revolution of the precessing vortex, the phase difference between the ends of the container slips by 2π . This process can be interpreted as a macroscopic manifestation of the ac Josephson effect [82,56]. The corresponding Josephson frequency is remarkably low, approximately 4 mHz.

(iv) Unimpeded by pinning on solid walls, it becomes possible to study interactions of vortex lines with different types of interfaces which can be prepared in the He systems. These interfaces include the free surface of the superfluid bath (i.e. the gas – liquid interface) [83], the superfluid – solid ^3He interface [84], the interfaces between ^3He and ^4He superfluids [76,85], and interfaces between the A and B phases in superfluid ^3He [86].

11 Conclusion

Although superflow and quantized vortex lines have been the essence of superfluid investigations since the start in the late nineteen forties, nevertheless uniform rotation has not become an important tool for generating vorticity in $^4\text{He-II}$, owing to the uncontrolled release of remanent vorticity. When the construction work of the first rotating nuclear demagnetization cryostat was started in 1978 it was feared that rotation might not prove a useful concept in ^3He superfluidity either. However, today we know that the Ω axis is as important in the study of the ^3He superfluids as the other experimental parameters H , P , or T , which together control the various order-parameter structures: Measurements on ^3He superfluids without access to rotation would be as limited as studies on superconductors without the possibility to turn on the magnetic field!

The central areas so far in superfluid ^3He work have been the identification of different topologically stable defect structures in the order-parameter field, the conditions and critical values which control their formation, and phase transitions between different structures as function of the external variables. For these questions the ^3He superfluids have been the most ideal system, owing to the large variability in its order-parameter response. Today the

largest collection of different theoretically characterized and experimentally identified quantized vortex structures are found in the ^3He superfluids. In the coming years ^3He work will focus more and more on making use of its ideal text-book-like properties, to employ the ^3He liquids as a model system in quantum field theory for the study of such varied questions as the physical vacuum, black hole, or inhomogeneity in the accelerating Universe. For many questions of this category working theoretical ^3He analogues have already been constructed [87].

References

1. A.J. Leggett: Rev. Mod. Phys. **47**, 331 (1975)
2. M.M. Salomaa, G.E. Volovik: Rev. Mod. Phys. **59**, 533 (1987)
3. V.M. Ruutu, Ü. Parts, M. Krusius: J. Low Temp. Phys. **103**, 331 (1996)
4. J.M. Karimäki, E.V. Thuneberg: Phys. Rev. B **60**, 15290 (1999)
5. M. Rice: Nature **396**, 627 (1998)
6. K. Ishida, H. Mukuda, Y. Kitaoka, K. Asayama, Z. Q. Mao, Y. Mori, Y. Maeno: Nature **396**, 658 (1998)
7. V.M. Ruutu, V.B. Eltsov, A.J. Gill, T.W.B. Kibble, M. Krusius, Yu.G. Makhlin, B. Plaçais, G.E. Volovik, Wen Xu: Nature **382**, 334 (1996); C. Bäuerle, Yu.M. Bunkov, S.N. Fisher, H. Godfrin, G.R. Pickett: Nature **382**, 332 (1996)
8. T.D. Bevan, A.J. Manninen, J.B. Cook, J.R. Hook, H.E. Hall, T. Vachaspati, G.E. Volovik: Nature **386**, 689 (1997)
9. D. Vollhardt, P. Wölfle: *The superfluid phases of He-3* (Taylor & Francis, London, 1990)
10. C.G. Callan, R. Dashen, D.J. Gross: Phys. Lett. **B 66**, 375 (1977)
11. V.A. Fateev, I.V. Frolov, A.S. Schwarz: Nucl. Phys. **B 154**, 1 (1979)
12. J.V. Steel, J.W. Negele: hep-lat/0007006
13. P.J. Hakonen, O.T. Ikkala, S.T. Ikkala: Phys. Rev. Lett. **49**, 1258 (1982)
14. R. Blaauwgeers, V.B. Eltsov, M. Krusius, J.J. Ruohio, R. Schanen, G.E. Volovik: Nature **404**, 471 (2000)
15. S.M. Girvin: Phys. Today **53**, N. 6, 39 (2000)
16. L.I. Burlachkov, N.B. Kopnin: Sov. Phys. JETP **65**, 630 (1987)
17. M.R. Matthews, B.P. Anderson, P.C. Haljan, D.S. Hall, C.E. Wieman, E.A. Cornell: Phys. Rev. Lett. **83**, 2498 (1999)
18. T.-L. Ho: Phys. Rev. Lett. **81**, 742 (1998)
19. T. Isoshima, M. Nakahara, T. Ohmi, K. Machida: Phys. Rev. A **61**, 63610-1 (2000)
20. K.P. Marzlin, W. Zhang, B.C. Sanders: preprint cond-mat/0003273
21. Ü. Parts, J.M. Karimäki, J.H. Koivuniemi, M. Krusius, V.M. Ruutu, E.V. Thuneberg, G.E. Volovik: Phys. Rev. Lett. **75**, 3320 (1995)
22. Ü. Parts, E.V. Thuneberg, G.E. Volovik, J.H. Koivuniemi, V.H. Ruutu, M. Heinilä, J.M. Karimäki, M. Krusius: Phys. Rev. Lett. **72**, 3839 (1994); E.V. Thuneberg: Physica B **210**, 287 (1995); M.T. Heinilä, G.E. Volovik, Physica B **210**, 300 (1995); Ü. Parts, V.M. Ruutu, J.H. Koivuniemi, M. Krusius, E.V. Thuneberg, G.E. Volovik: Physica B **210**, 311 (1995)

23. P.G. Saffman: *Vortex dynamics* (Cambridge Univ. Press, Cambridge, UK, 1997); H. Lamb: *Hydrodynamics* (Dover Publ., New York, 1932)
24. L. Onsager: unpublished, see F. London, *Superfluids*, Vol II (Wiley, New York), p 151; see also Ref. [59]
25. H. London, in *Report of Intern. Conf. on Fund. Particles and Low Temp.*, Vol II, (Physical Society, London, 1946), p. 48
26. L. Landau, E. Lifshitz: Dokl. Akad. Nauk. **100**, 669 (1955)
27. Ü. Parts, J.H. Koivuniemi, M. Krusius, V.M. Ruutu, E.V. Thuneberg, G.E. Volovik: Pis'ma ZETF **59**, 816 (1994) [JETP Lett. **59**, 851 (1994)]
28. M. Sigrist, T.M. Rice, K. Ueda: Phys. Rev. Lett. **63**, 1727 (1989)
29. E. Shung, T.F. Rosenbaum, M. Sigrist: Phys. Rev. Lett. **80**, 1078 (1998)
30. G.E. Volovik, L.P. Gor'kov: Sov. Phys. JETP **61**, 843 (1985)
31. F. Pardo, F. de la Cruz, P.L. Gammel, E. Bucher, D.J. Bishop, Nature **396**, 348 (1998)
32. G.E. Volovik, V.P. Mineev: JETP Lett. **24**, 561 (1976)
33. V. Geshkenbein, A. Larkin, A. Barone: Phys. Rev. B **36**, 235 (1987)
34. J.R. Kirtley, C.C. Tsuei, M. Rupp, J.Z. Sun, L.S. Yu-Jahnes, A. Gupta, M.B. Ketchen, K.A. Moler, M. Bhushan: Phys. Rev. Lett. **76**, 1336 (1996)
35. U. Leonhardt, G.E. Volovik: Pis'ma ZhETF **72**, 66 (2000) [JETP Lett. **72**, 46 (2000)]
36. A.S. Schwarz: Nucl. Phys. B **208**, 141 (1982)
37. Z.K. Silagadze: preprint hep-ph/0002255; Mod. Phys. Lett. **A14**, 2321 (1999)
38. H.-Y. Kee, Y.B. Kim, K. Maki: Phys. Rev. B **62**, R9275 (2000)
39. G.E. Volovik: Proc. Natl. Acad. Sc. USA **97**, 2431 (2000)
40. G.E. Volovik, L.P. Gor'kov: JETP Lett. **39**, 674 (1984)
41. M. Sigrist, D.B. Bailey, R.B. Laughlin: Phys. Rev. Lett. **74**, 3249 (1995)
42. G.E. Volovik: Pis'ma ZhETF **58**, 457 (1993) [JETP Lett. **58**, 469 (1993)]
43. O.T. Ikkala, G.E. Volovik, P.J. Hakonen, Yu.M. Bunkov, S.T. Islander, G.A. Kharadze: Pis'ma Zh. Eksp. Teor. Fiz. **35**, 338 (1982) [JETP Lett. **35**, 416 (1982)]
44. M.M. Salomaa, G.E. Volovik: Phys. Rev. Lett. **51**, 2040 (1983)
45. P.J. Hakonen, M. Krusius, M.M. Salomaa, J.T. Simola, Yu.M. Bunkov, V.P. Mineev, G.E. Volovik: Phys. Rev. Lett. **51**, 1362 (1983)
46. E.V. Thuneberg: Phys. Rev. Lett. **56**, 359 (1986); M.M. Salomaa, G.E. Volovik: *ibid.* **56**, 363 (1986); E.V. Thuneberg: Phys. Rev. B **33**, 5124 (1986)
47. On $SO(5)$ model see e.g. N.A. Mortensen, H. M. Ronnow, H. Bruus, P. Hedegard: Phys. Rev. B **62**, 8703 (2000) and references therein
48. D.P. Arovas, A. J. Berlinsky, C. Kallin, S.-C. Zhang: Phys. Rev. Lett. **79**, 2871 (1997); S. Alama, A.J. Berlinsky, L. Bronsard, T. Giorgi: Phys. Rev. B **60**, 6901 (1999)
49. T.A. Tokuyasu, D.W. Hess, J.A. Sauls: Phys. Rev. B **41**, 8891 (1990); J.A. Sauls: Adv. Phys. **43**, 113 (1994); N. Lütke-Entrup, R. Blaauwgeers, A. Huxley, S. Kambe, M. Krusius, P. Mathieu, B. Plaçais, Y. Simon: to be published
50. Y. Kondo, J.S. Korhonen, M. Krusius, V.V. Dmitriev, Yu. M. Mukharskiy, E.B. Sonin, G.E. Volovik: Phys. Rev. Lett. **67**, 81 (1991)
51. M.M. Salomaa, G.E. Volovik: J. Low Temp. Phys. **74**, 319 (1989)
52. G.E. Volovik: Pis'ma ZETF **52**, 972 (1990) [JETP Lett. **52**, 358 (1990)]
53. I.A. Luk'yanchuk, M.E. Zhitomirsky: Superconductivity Review **1**, 207 (1995)
54. B.W. Hoogenboom, M. Kugler, B. Revaz, I. Maggio-Aprile, O. Fischer, Ch. Renner: Phys. Rev. B **62**, 9179 (2000)

55. E. Varoquaux, O. Avenel: *Physica B* **197**, 306 (1994)
56. R.E. Packard: *Rev. Mod. Phys.* **70**, 641 (1998)
57. J.C. Davis, J. Steinhauer, K. Schwab, Yu.M. Mukharsky, A. Amar, Y. Sasaki, R.E. Packard: *Phys. Rev. Lett.* **69**, 323 (1992); G.G. Ihas, O. Avenel, R. Aarts, R. Salmelin, E. Varoquaux, *Phys. Rev. Lett.* **69**, 327 (1992); *ibid.* **70**, 2114 (1993)
58. Ü. Parts, V.M. Ruutu, J.H. Koivuniemi, Yu.M. Bunkov, V.V. Dmitriev, M. Fogelström, M. Huebner, Y. Kondo, N.B. Kopnin, J.S. Korhonen, M. Krusius, O.V. Lounasmaa, P.I. Soininen, G.E. Volovik: *Europhys. Lett.* **31**, 449 (1995); *J. Low Temp. Phys.* **107**, 93 (1997)
59. R.J. Donnelly: *Quantized vortices in He-II* (Cambridge Univ. Press, Cambridge, UK, 1991)
60. D. Vollhardt, K. Maki, N. Schopohl: *J. Low Temp. Phys.* **39**, 79 (1980); H. Kleinert, *J. Low Temp. Phys.* **39**, 451 (1980)
61. V.M. Ruutu, J. Kopu, M. Krusius, Ü. Parts, B. Plaçais, E.V. Thuneberg, W. Xu: *Phys. Rev. Lett.* **79**, 5058 (1997)
62. J. Kopu, R. Hänninen, and E.V. Thuneberg, *Phys. Rev. B* **62**, 12374 (2000)
63. R. Blaauwgeers, V.B. Eltsov, M. Krusius, J.J. Ruohio, R. Schanen: in *Superfluid turbulence and quantized vortex dynamics*, ed. C. Barenghi (Springer Verlag, Berlin, 2001)
64. T. Kita, *Phys. Rev. Lett.* **83**, 1846 (1999)
65. V.B. Eltsov, R. Blaauwgeers, N.B. Kopnin, M. Krusius, J.J. Ruohio, R. Schanen, E.V. Thuneberg: to be published
66. T.W.B. Kibble, *J. Phys. A* **9**, 1387 (1976)
67. W.H. Zurek, *Nature* **317**, 505 (1985)
68. V.B. Eltsov, M. Krusius, G.E. Volovik: in *Prog. Low Temp. Phys.*, ed. W.P. Halperin, Vol. XV (Elsevier Science Publ., Amsterdam, 2001), preprint cond-mat/9809125
69. T.W.B. Kibble and G.E. Volovik, *JETP Lett.* **65**, 102 (1997)
70. J. Dziarmaga, P. Laguna, W.H. Zurek: *Phys. Rev. Lett.* **82**, 4749 (1999)
71. N.B. Kopnin, E.V. Thuneberg: *Phys. Rev. Lett.* **83**, 116 (1999)
72. V.M. Ruutu, V.B. Eltsov, M. Krusius, Yu.G. Makhlin, B. Plaçais, G.E. Volovik: *Phys. Rev. Lett.* **80**, 1465 (1998)
73. I.S. Aranson, N.B. Kopnin, V.M. Vinokur: *Phys. Rev. Lett.* **83**, 2600 (1999)
74. V.B. Eltsov, T.W.B. Kibble, M. Krusius, V.M.H. Ruutu, G.E. Volovik: *Phys. Rev. Lett.* **85**, 4739 (2000).
75. S.G. Hedge, W.I. Glaberson: *Phys. Rev. Lett.* **45**, 190 (1980); W.I. Glaberson, R.J. Donnelly: in *Prog. Low Temp. Phys.*, ed. D.F. Brewer, Vol. IX, p. 81 (Elsevier Science Publ., Amsterdam, 1986)
76. M. Krusius, J.S. Korhonen, Y. Kondo, E.B. Sonin: *Phys. Rev. B* **47**, 15113 (1993)
77. T.D. Bevan, A.J. Manninen, J.B. Cook, H. Alles, J.R. Hook, H.E. Hall: *J. Low Temp. Phys.* **109**, 423 (1997)
78. N.B. Kopnin, G.E. Volovik, Ü. Parts: *Europhys. Lett.* **32**, 651 (1995)
79. M. Stone, *Phys. Rev. B* **61**, 11780 – 11786 (2000)
80. W.F. Vinen, *Proc. Royal Soc. London A* **260**, 218 (1961)
81. R.J. Zieve, Yu.M. Mukharsky, J.D. Close, J.C. Davis, R.E. Packard: *J. Low Temp. Phys.* **91**, 315 (1991); *Phys. Rev. Lett.* **68**, 1327 (1992)
82. T.Sh. Misirpashaev, G.E. Volovik, *Pis'ma Zh. Exp. Teor. Fiz.* **56**, 40 (1992) [*JETP Lett.* **56**, 41 (1992)]

83. E.B. Sonin, A.J. Manninen: Phys. Rev. Lett. **70**, 2585 (1993)
84. A.Ya. Parshin: Physica B **210**, 383 (1995)
85. Y. Kondo, J.S. Korhonen, M. Krusius: Physica B **169**, 533 (1991)
86. Ü. Parts, Y. Kondo, J.S. Korhonen, M. Krusius, E.V. Thuneberg: Phys. Rev. Lett. **71**, 2951 (1993)
87. G.E. Volovik: Phys. Rep., to be published (2001); preprint gr-qc/0005091